Mesoporous titanium niobium nitrides supported Pt nanoparticles for highly selective and sensitive formaldehyde sensing

Chaozhu Huang[b,c], Samira Adimi[a], Dongliang Liu[b], Haichuan Guo[b], Tiju Thomas[d], J. Paul Attfield[e], Shengping Ruan[a], Fengdong Qu[b] and Minghui Yang[b,c*]*

[a]State Key Laboratory on Integrated Optoelectronics, College of Electronic Science and Engineering, Jilin University, Changchun, 130012, China

[b]Ningbo Institute of Materials Technology and Engineering, Chinese Academy of Sciences, Ningbo 315201, China.

[c]Center of Materials Science and Optoelectronics Engineering, University of Chinese Academy of Sciences, Beijing 100049, China.

[d]Department of Metallurgical and Materials Engineering, Indian Institute of Technology Madras, Adyar, Chennai-600036, India

[e]Centre for Science at Extreme Conditions and School of Chemistry, University of Edinburgh,King's Buildings, Mayfield Road, Edinburgh, EH93JZ, United Kingdom.

E-mail: fqu@nimte.ac.cn (F.Q.); myang@nimte.ac.cn (M.Y.)

Computational methodology: DFT calculations were performed with the Dmol3 package code in Material Studio 8.0. the double numerical plus polarization (DNP) basis set and the generalized-gradient approximation (GGA) with the Perdew-Burke-Emzerhof (PBE) were employed to obtain all the results reported below[1, 2]. In order to avoid the interaction between adjacent cells, a vacuum slab of 15 Å was established. The core treatment was set as Effective Core Potential to manage the interaction between the nucleus and valence electron, whereas the Brillouin zone k-point sampling was performed in 2×2×1 Monkhorst-Pack mesh. The energy tolerance accuracy, maximum force, and displacement were set as 10^{-5} Ha, 2×10^{-2} Ha/Å, 3.7 Å and 5×10^{-2} Å, respectively. For static electronic structure calculations, self-consistent loop energy of 10^{-5} Ha and smearing of 0.005 Ha were employed to ensure the accurate results of total energy[3].

The formation energy (E_{for}) between Pt and support was calculated by the following equation:

$E_{for} = E_{Pt/support} - (E_{Pt} + E_{support})$

$E_{Pt/support}$, E_{Pt} and $E_{support}$ are the total energies of the total energy of the support combined with Pt, Pt and support, respectively.

Gas distribution formula

For vapors:

$$V_1 = \frac{V \times C \times M}{22.4 \times d \times P} \times \frac{273 + T_R}{273 + T_B} \times 10^{-9}$$

For gases:

$$V_1 = V \times C \times \frac{273 + T_R}{273 + T_B} \times 10^{-6}$$

V_1 represents the volume of liquid vapor or high purity gas to be injected during gas distribution (unit: ml), V represents the volume of test bottle (unit: ml), M represents the molecular weight of the prepared liquid, D represents the specific gravity (unit: g/cm^3), P represents the purity (liquid), T_R represents the ambient temperature, T_B represents the temperature in the test bottle (unit: °C), C represents the concentration of liquid vapor to be configured for the experiment (unit: ppm).

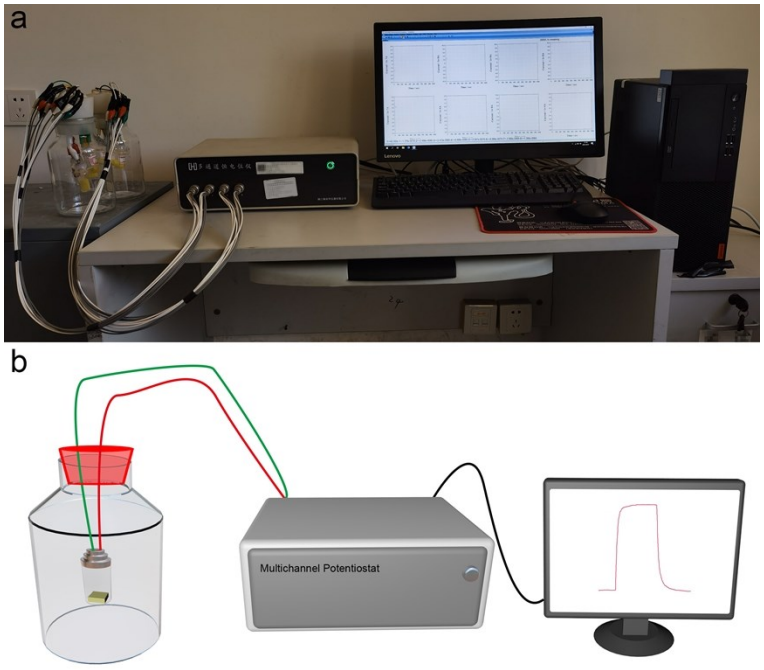

Supplementary Figure S1. a) The real picture and b) schematic diagram of the test system.

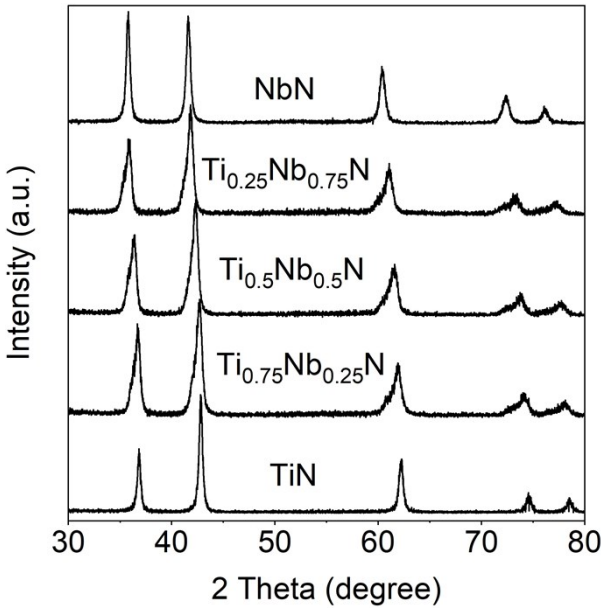

Supplementary Figure S2. XRD pattern of $Ti_xNb_{1-x}N$.

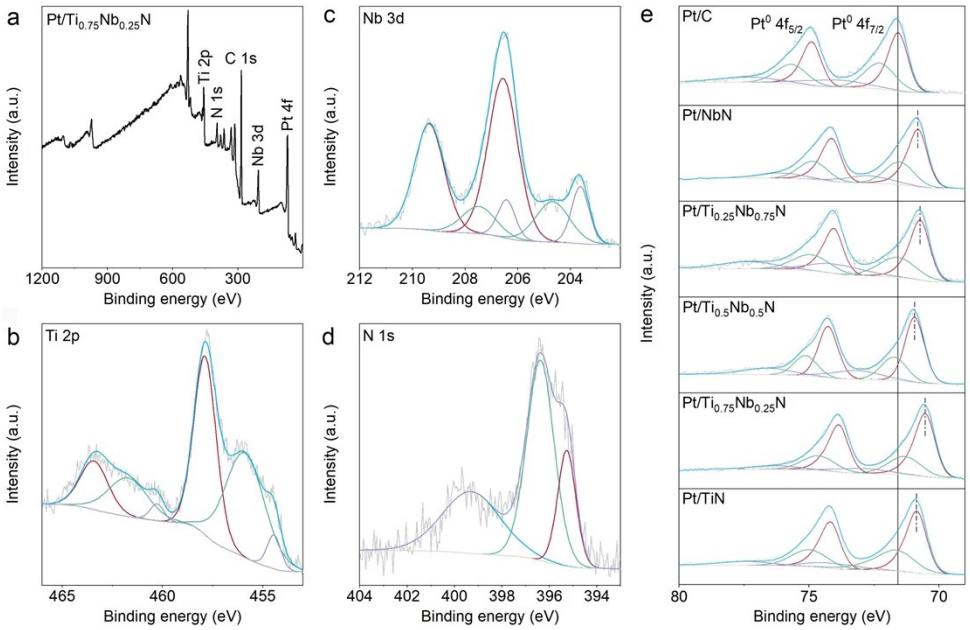

Supplementary Figure S3. XPS spectra a) Wide-range, b) Ti 2p region, c) Nb 3d region and d) N 1s region spectra of $Pt/Ti_{0.75}Nb_{0.25}N$ NPs, e) Pt 4f region spectra of commercial Pt/C and $Pt/Ti_xNb_{1-x}N$.

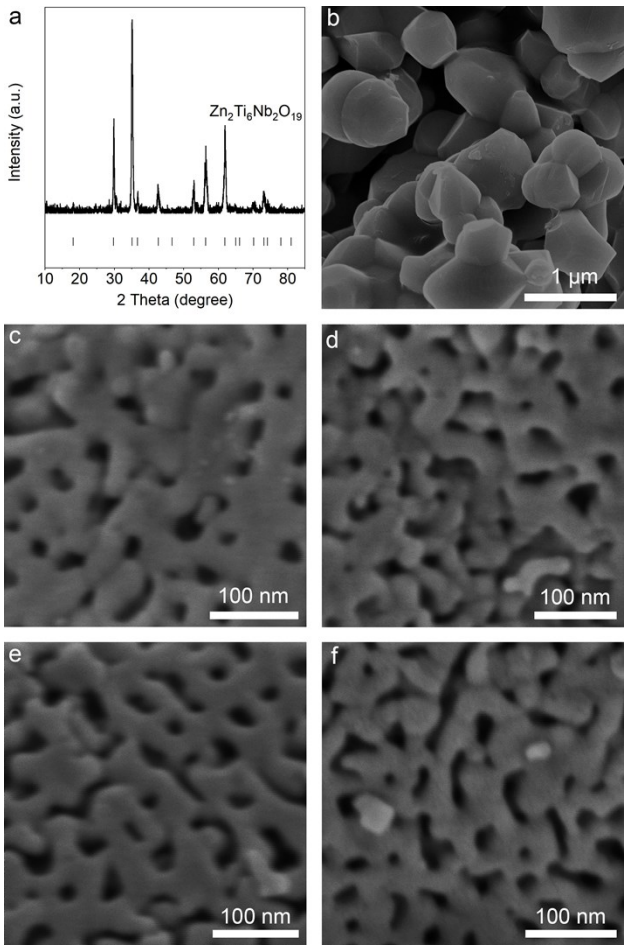

Supplementary Figure S4. a) XRD pattern and b) SEM images of molten precursor. The SEM images of c) NbN, d) $Ti_{0.25}Nb_{0.75}N$, e) $Ti_{0.5}Nb_{0.5}N$ and (f) TiN

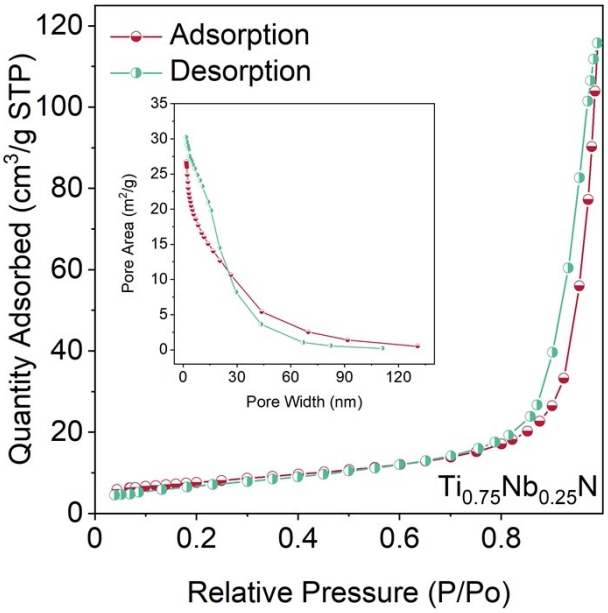

Supplementary Figure S5. N_2 adsorption-desorption isotherm and pore size distribution of $Ti_{0.75}Nb_{0.25}N$.

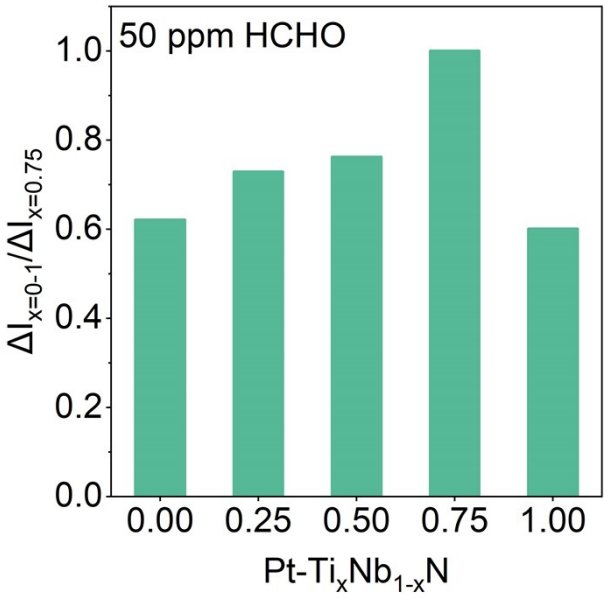

Supplementary Figure S6. The ratio of the *ΔI* of Pt/$Ti_xNb_{1-x}N$ sensor to that of Pt/$Ti_{0.75}Nb_{0.25}N$ sensor in 50 ppm formaldehyde.

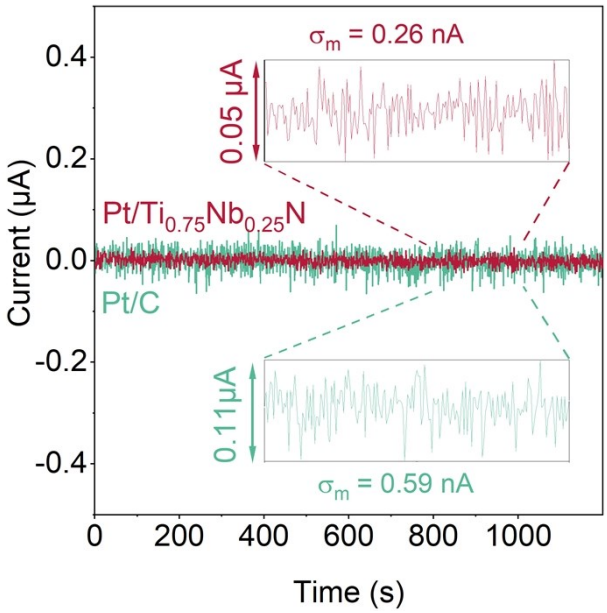

Supplementary Figure S7. Current baseline of $Pt/Ti_{0.75}Nb_{0.25}N$ and commercial Pt/C sensor in air for 20 min. The insets show zoomed-in regions spanning 200 s.

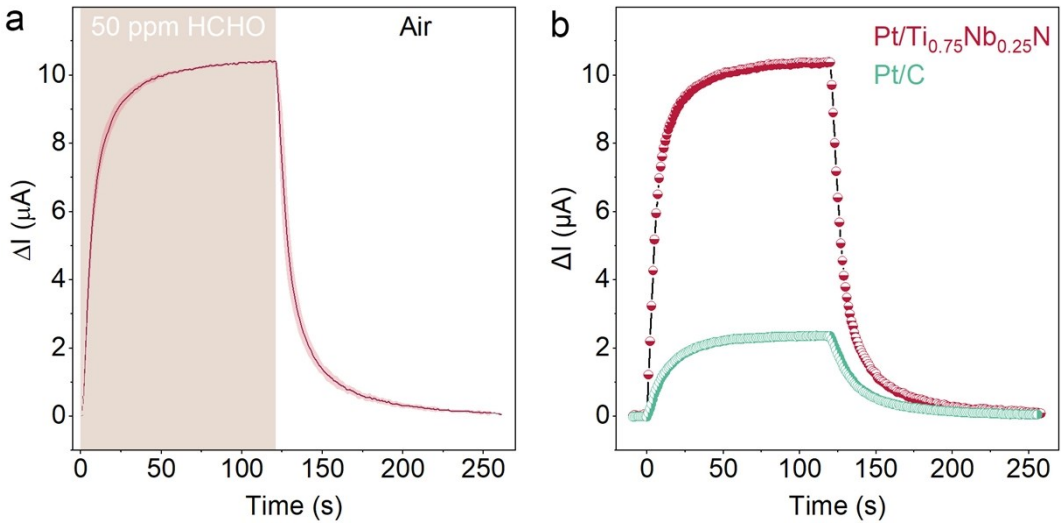

Supplementary Figure S8. a) Average change in response (ΔI) of $Pt/Ti_{0.75}Nb_{0.25}N$ sensor to 50 ppm formaldehyde gas. Shaded areas represent standard deviations (SDs, n=6). b) Average real-time response of $Pt/Ti_{0.75}Nb_{0.25}N$ and Pt/C-based sensor to 50 ppm formaldehyde at fresh and 2 months later.

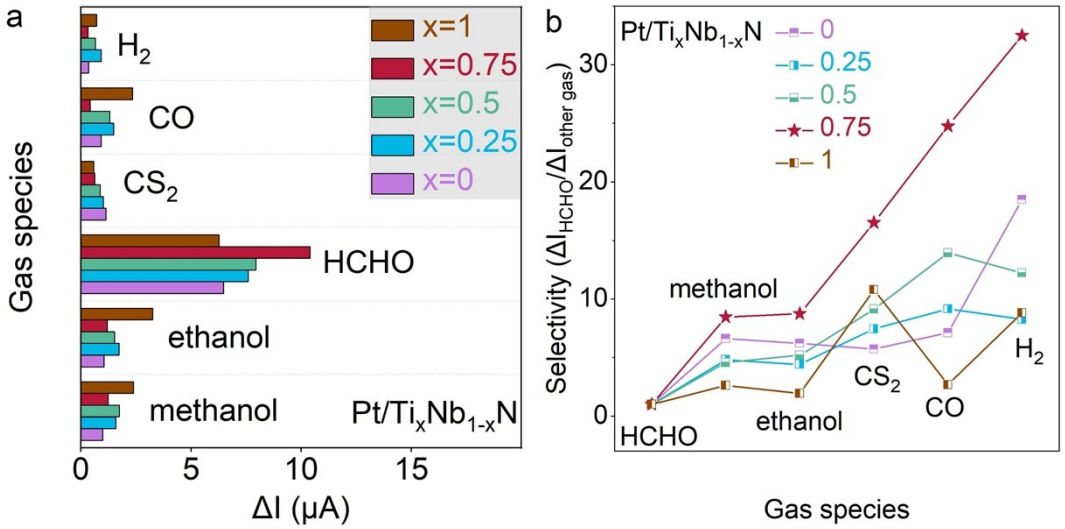

Supplementary Figure S9.a) Selectivity and b) selectivity improvements of $Pt/Ti_xNb_{1-x}N$ (x=0, 0.25, 0.5, 0.75, 1) sensor toward various analyte gases.

Figure S9a shows the response of $Pt/Ti_xNb_{1-x}N$ on 50 ppm formaldehyde (HCHO), methanol (CH_3OH), ethanol (C_2H_5OH), hydrogen (H_2), carbon monoxide (CO) and carbon disulfide (CS_2) under the same conditions. Although all the sensors exhibit selectivity for formaldehyde, $Pt/Ti_{0.75}Nb_{0.25}N$ has the highest formaldehyde response. Compared to other sensors, the response of $Pt/Ti_{0.75}Nb_{0.25}N$ to other interfering gases is effectively suppressed. Adjusting the composition of ternary nitrides can change the surface chemical properties of nitrides and affect the catalytic activity for gas reaction.[4, 5] When the atomic ratio of Ti to Nb is adjusted to 3:1, the catalytic activity of the gas sensing catalyst for formaldehyde is significantly enhanced. This may be due to the synergistic effect of Pt and $Ti_{0.75}Nb_{0.25}N$, which makes the catalyst show the best catalytic activity for formaldehyde. As shown in Figure S9b, we confirm that $Pt/Ti_{0.75}Nb_{0.25}N$ is the best composition of $Ti_xNb_{1-x}N$ offering selectivity for sensing formaldehyde. This is determined by calculating the selectivity ($\Delta I_{HCHO}/\Delta I_{other\ gas}$) of the sensor. Therefore, $Ti_{0.75}Nb_{0.25}N$is selected as catalyst support to replace carbon black for improvement in the performance of the sensor.

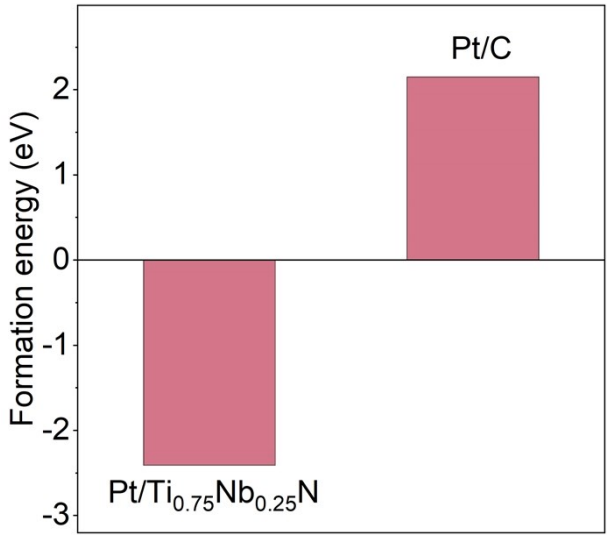

Supplementary Figure S10. Formation energy of $Pt/Ti_{0.75}Nb_{0.25}N$ and Pt/C.

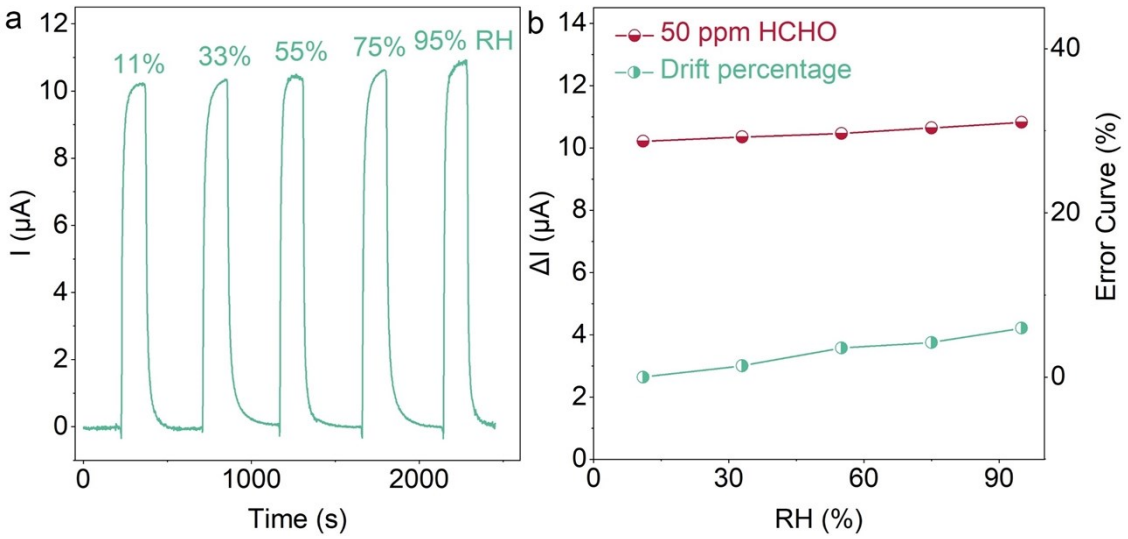

Supplementary Figure S11. The influence of relative humidity (RH) on the gas sensing performance of the sensor. a) Transient response and b) response current and drift percentage under different RH.

Supplementary Table S1. The results of as prepared $Ti_xNb_{1-x}N$

Sample	Atomic ratio of raw materials (Ti:Nb)	The results of ICP (Ti:Nb)
NbN	0:1	0:1
$Ti_{0.25}Nb_{0.75}N$	1:3	1:2.89
$Ti_{0.5}Nb_{0.5}N$	1:1	1:1.04
$Ti_{0.75}Nb_{0.25}N$	3:1	2.92:1
TiN	1:0	1:0

Supplementary Table S2. The summary of gas sensing devices for formaldehyde sensing characteristics reported recently

Sensing electrode	Working conditions	Sensing signal	Typical response	Sensitivity	T_{res}/T_{reco} time (s)	Sensitivity drift	References
$Pt/Ti_{0.75}Nb_{0.25}N$	RT	Current	10.42μA (50 ppm)	0.208 μA/ppm	14/19	1%/2 months	This work
Pt/C (JM)	RT	Current	3.01μA (100 ppm)	0.058 μA/ppm	38/57	43%/2 months	Johnson Matthey
$Ni–In_2O_3/WS_2$	RT	Resistance	32 (20 ppm)	14.84/ppm	76/123	~3%/2 months	[6]
Ag@Pt@ZnO	280 °C	Resistance	0.26 (240 ppb)	/	162/225	~5%/42 days	[7]
Au/In_2O_3	100 °C	Resistance	85.67 (50 ppm)	1465/ppm	25/198	~5%/1 month	[8]
Co-doped In_2O_3	130 °C	Resistance	23.2 (10 ppm)	~2.5/ppm	60/12	~10%/30 days	[9]
6%-Ag/$Ni_{5.0}$ In_2O_3	160 °C	Resistance	74.01 (50 ppm)	/	1.45/58.2	3%/21 days	[10]
$CdO/CdGa_2O_4$	110 °C	Resistance	1.5 (10 ppm)	4.454/ppm	10/120	10%/45 days	[11]
2D GO/SnO_2	60°C	Resistance	2275.7 (100 ppm)	/	81.3/33.7	/	[12]
La_2O_3-SnO_2-Sn_3O_4	220 °C	Resistance	117.29 (100 ppm)	0.00125/ppb	3/3	/	[13]
PEI/BC	200 MHZ	Frequency shift	35600 HZ (10 ppm)	5.8 Hz/ppb	34/28	~5%/32 days	[14]
PDA/ZnO	RT	Enthalpy (ΔH^o)	~800 HZ (30 ppm)	0.46 Hz/ppb	/	/	[15]
7.5 wt.% K-CGO	120 °C	Resistance	90 (10 ppm)	7.021/ppm	1/62	~15%/30 days	[16]
PdAu/SnO_2	110 °C	Resistance	125 (100 ppm)	111.3In C	68/32	/	[17]
5% Ca-In_2O_3	130 °C	Resistance	116 (100 ppm)	1.2/ppm	116/328	~35%/30 days	[18]
H-SnO2@rGO	130 °C	Resistance	435 (10 ppm)	159/ppm	/	~3%/10 days	[19]
Pr-$BiFeO_3$	190 °C	Resistance	30.1 (100 ppm)	~0.25/ppm	17/19	~10%/28 days	[20]
NiO/$NiFe_2O_4$	240 °C	Resistance	27 (50 ppm)	/	9/3	~3%/30 days	[21]
Sn_3O_4/rGO	150 °C	Resistance	44 (100 ppm)	0.3754/ppm	4/125	~6%/56 days	[22]
$LaFeO_3$	125 °C	Resistance	116 (5 ppm)	1.37/ppm	3.8/25.6	4%/15 weeks	[23]
PdO-ZnO/$ZnCo_2O_4$	139 °C	Resistance	26.5(100 ppm)	0.32/ppm	12/22	~13%/90 days	[24]
Sn-MOFs	120 °C	Resistance	882(2 ppm)	/	19/~25	~20%/8 days	[25]
SnO_2/ZnO	200 °C	Resistance	38.2(20 ppm)	0.5056/ppm	27/89	~12%/7 months	[26]

References

1. H. Cui, G. Zhang, X. Zhang and J. Tang, *Nanoscale Advances*, 2019, **1**, 772-780.
2. H. Cui, X. Zhang, G. Zhang and J. Tang, *Applied Surface Science*, 2019, **470**, 1035-1042.
3. W. Ju, T. Li, X. Su, H. Li, X. Li and D. Ma, *Phys Chem Chem Phys*, 2017, **19**, 20735-20748.
4. Z. Cui, R. G. Burns and F. J. DiSalvo, *Chemistry of Materials*, 2013, **25**, 3782-3784.
5. M. Yang, A. R. Van Wassen, R. Guarecuco, H. D. Abruna and F. J. DiSalvo, *Chem Commun (Camb)*, 2013, **49**, 10853-10855.
6. D. Zhang, Y. Cao, Z. Yang and J. Wu, *ACS Appl Mater Interfaces*, 2020, **12**, 11979-11989.
7. D. Xu, P. Xu, X. Wang, Y. Chen, H. Yu, D. Zheng and X. Li, *ACS Appl Mater Interfaces*, 2020, **12**, 8091-8097.
8. F. Gu, M. Di, D. Han, S. Hong and Z. Wang, *ACS Sens*, 2020, **5**, 2611-2619.
9. Z. Wang, C. Hou, Q. De, F. Gu and D. Han, *ACS Sens*, 2018, **3**, 468-475.
10. X. Zhang, D. Song, Q. Liu, R. Chen, J. Hou, J. Liu, H. Zhang, J. Yu, P. Liu and J. Wang, *Journal of Materials Chemistry C*, 2019, **7**, 7219-7229.
11. H. Chen, L. Sun, G.-D. Li and X. Zou, *Chemistry of Materials*, 2018, **30**, 2018-2027.
12. D. Wang, L. Tian, H. Li, K. Wan, X. Yu, P. Wang, A. Chen, X. Wang and J. Yang, *ACS Appl Mater Interfaces*, 2019, **11**, 12808-12818.
13. H. Yu, J. Li, W. Luo, Z. Li, Y. Tian, Z. Yang, X. Gao and H. Liu, *Applied Surface Science*, 2020, **513**.
14. J. L. Wang, Y. J. Guo, G. D. Long, Y. L. Tang, Q. B. Tang, X. T. Zu, J. Y. Ma, B. Du, H. Torun and Y. Q. Fu, *J Hazard Mater*, 2020, **388**, 121743.
15. D. Yan, P. Xu, Q. Xiang, H. Mou, J. Xu, W. Wen, X. Li and Y. Zhang, *Journal of Materials Chemistry A*, 2016, **4**, 3487-3493.
16. Q. Liang, X. Qu, N. Bai, H. Chen, X. Zou and G. D. Li, *J Hazard Mater*, 2020, **400**, 123301.
17. G. Li, Z. Cheng, Q. Xiang, L. Yan, X. Wang and J. Xu, *Sensors and Actuators B: Chemical*, 2019, **283**, 590-601.
18. Q. Liang, X. Zou, H. Chen, M. Fan and G.-D. Li, *Sensors and Actuators B: Chemical*, 2020, **304**.
19. J. Hu, M. Chen, Q. Rong, Y. Zhang, H. Wang, D. Zhang, X. Zhao, S. Zhou, B. Zi, J. Zhao, J. Zhang, Z. Zhu and Q. Liu, *Sensors and Actuators B: Chemical*, 2020, **307**.
20. Y. Tie, S. Y. Ma, S. T. Pei, Q. X. Zhang, K. M. Zhu, R. Zhang, X. H. Xu, T. Han and W. W. Liu, *Sensors and Actuators B: Chemical*, 2020, **308**.
21. Y. Xu, X. Tian, Y. Fan and Y. Sun, *Sensors and Actuators B: Chemical*, 2020, **309**.
22. F. Yin, Y. Li, W. Yue, S. Gao, C. Zhang and Z. Chen, *Sensors and Actuators B: Chemical*, 2020, **312**.
23. K. Yang, J. Ma, X. Qiao, Y. Cui, L. Jia and H. Wang, *Sensors and Actuators B: Chemical*, 2020, **313**.
24. N. Zhang, Y. Lu, Y. Fan, J. Zhou, X. Li, S. Adimi, C. Liu and S. Ruan, *Sensors and Actuators B: Chemical*, 2020, **315**.
25. B. J. Wang, S. Y. Ma, S. T. Pei, X. L. Xu, P. F. Cao, J. L. Zhang, R. Zhang, X. H. Xu and T. Han, *Sensors and Actuators B: Chemical*, 2020, **321**.
26. C. Lou, C. Yang, W. Zheng, X. Liu and J. Zhang, *Sensors and Actuators B: Chemical*, 2021, **329**.